論文 / 著書情報
Article / Book Information

Title	CFD Analysis of Water Droplet Behavior in Axial Flow Compressor
Authors	Makoto Koizumi, Motoaki Utamura, Toyohiko Yano, Susumu Nakano, Takanori Shibata, Chihiro Myoren
Citation	International Journal of Gas Turbine, Propulsion and Power Systems, Vol. 8, No. 3, pp. 12-19
Pub. date	2016, 12

CFD Analysis of Water Droplet Behavior in Axial Flow Compressor

Makoto Koizumi[1], Motoaki Utamura[1], Toyohiko Yano[1], Susumu Nakano[2], Takanori Shibata[2], Chihiro Myoren[2]

[1] Research Laboratory for Nuclear Reactors, Tokyo Institute of Technology, Tokyo, Japan
2-12-1, Ookayama, Meguro-ku, Tokyo 152-8550, Japan
E-mail: mkoizumi@nr.titech.ac.jp
[2] Mitsubishi Hitachi Power Systems, Ltd.

ABSTRACT

A numerical model is developed to characterize erosion caused by water droplets impinging against rotor blades at the first stage of an axial flow compressor. Analyses assume a gas turbine operating with an inlet fogging system. The change in the water droplet size attributable to break-up and evaporation during flight is considered. Numerical calculations are executed using a commercial code in a two-dimensional computational domain including an inlet guide vane, rotor, and stator.

The calculated erosion depth shows good agreement with that obtained from empirical correlation in the case without a break-up model. Results show that the break-up occurs over a certain rotor speed, leading to marked reduction of the erosion depth. The choice of the droplet critical Weber number determines the rotor velocity which maximizes the erosion depth. Secondary droplets discharged from the trailing edge of IGV (Inlet Guide Vane) affect erosion more than primary droplets, although their mass flow is smaller.

NOMENCLATURE

a	Eq. (2) [mm]
b	Eq. (3) [mm/hr]
C	constant in Eq. (8)[-]
D	droplet diameter [mm]
$D32$	Sauter Mean Diameter [mm]
E_{st}	erosion depth [mm]
G	mass flow rate of water droplet [kg/s]
H	Vickers hardness [-]
L	number of parcels impacting on blade [1]
l	l-th parcel number [-]
M	relative Mach number [-]
m	number of droplets in a parcel [1]
N	number density of collisions [1/(mm^{2}hr)]
P	number of parcels emitted [1/s]
r	radius of droplet [mm]
t	sampling time [hr], break-up time [s]
u	droplet velocity relative to air [m/s]
V	impact velocity [m/s]
V_n	normal component of V [m/s]
We	Weber number ($\equiv \rho_g u^2 D/\sigma$) [-]
We,cr	critical Weber number [-]

Greek letters

ν	kinematic viscosity of water droplet [m^2/s]
ρ	density [kg/m^3]
σ	surface tension [N/m]
τ	compressor operation time [hr]

Subscripts

d	droplet
g	humid air (gas)
l	liquid, parcel number

Manuscript Received on March 18, 2016
Review Completed on November 17, 2016

INTRODUCTION

Inlet fogging technology, which is widely used for power augmentation of gas turbines during hot seasons, injects finely atomized water droplets into intake air and then cools the air by the latent heat of water evaporation. For fogging operations where injected water exceeds the amount to saturate the incoming air, some injected droplets enter the compressor. Aircraft engines also experience ingestion of water droplets into the compressor during flight in rain. Some attach to internal structures such as struts and inlet guide vanes, where they form films flowing on the surfaces. The film flow then splashes at the trailing edge and reproduces secondary water droplets that are often larger than the primary ones entering the compressor. Some primary and secondary droplets might hit the rotor blade and cause erosion of the material.

Experimental studies have examined water impingement erosion. Parametric effects have been clarified. Tsubouchi et al. [1] conducted elaborate experiments simulating erosion by condensate anticipated in low-pressure steam turbines. Typical water droplet diameters were 30 μm. Itoh et al. [2] derived an empirical correlation for erosion depth based on a parametric experiment using larger droplets of 100–270 μm diameter. Hattori et al. [3] studied effects of water droplet impact angles on erosion, reporting that the erosion depth is a function of the normal component of impact velocity. Uchida et al. [4] conducted a basic experiment to assess secondary droplet formation at the trailing edge of an Inlet guide vane (IGV). Matsuzaki et al. [5] studied water splash behavior from a plate placed parallel to the air flow, deriving an empirical correlation of the critical Weber number as a function of the Mach number. Nevertheless, few numerical studies have been reported. Suzuki et al. [6, 7] reported numerical simulations of water droplet impact against a compressor rotor blade, assuming nonvolatile, single-diameter droplets, and using solid particle approximation for water droplets. Therefore, the study did not consider changing droplet diameter during flight caused by break-up or evaporation.

Using a newly developed algorithm, this study numerically investigated the effects of the break-up of flying droplets and droplet size distributions on erosion.

NUMERICAL MODEL

Outline

Air flow containing water droplets in an axial flow compressor was solved in two dimensions using commercial CFD ANSYS Fluent 16.1. An Euler–Lagrange dispersed particle model was used to compute the two-phase flows: air is the continuous phase; water droplets are the dispersed phase. Air was approximated to ideal gas. Conservations of mass, momentum and energy were discretized by control volume method. Advection terms were solved by second order upwind. Implicit time integration was applied to discretized equation systems. To consider turbulence standard k-ε model with skin friction formula near blade surface was used. The velocity, turbulence, and other parameters were computed first in an Euler system. Then the traces of water droplets were obtained by integration in a Lagrange framework after considering the turbulence diffusion and aerodynamic force from the continuous phase. The particles were approximated by spherical shape and coefficient of drag force was calculated as function of Reynolds number. Fluent adopts parcel approximation, which treats a group of droplets as having identical properties instead of treating them as individual droplets, thereby obviating the need for huge computation resources. The accuracy of Fluent built into the evaporation model was confirmed by Hamdani et al. [8].

For erosion by water droplet impingement, the first stage rotor is the primary concern. To model a flow field around the rotor accurately, the computational domain was configured with a set of IGV, rotor and stator at the first stage of the axial flow compressor. In doing so, the water droplets trapped by IGV and the rate of secondary droplet generation at the trailing edge of IGV were evaluated. Then the contributions of primary and secondary droplets on rotor erosion were identified. Figure 1 shows the computational domain. Figure 2 shows the computational mesh around the leading edge of a rotor. Quadrilateral elements were used in the domain. The turbulence boundary layer was considered with y^+ of the first blade surface element set larger than 30. It was confirmed by steady state calculation. A sliding mesh was applied to the rotor sub-domain.

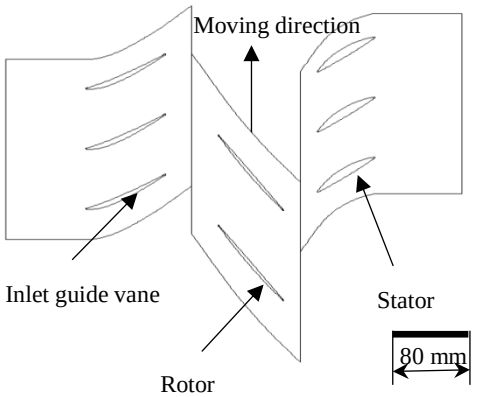

Fig. 1 Computational domain.

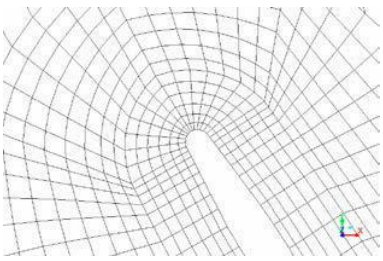

Fig. 2 Computational mesh near the rotor leading edge.

The total number of cells is 40 thousand. The time step was chosen such that the distance of rotor movement in a time step coincides with the size of computational element on the interface between the rotor and stator. Air flows through the whole domain from left to right in 410 cycles. The rotor moves one pitch in 40. An empirical erosion correlation was applied.

Simulation parameters

As the boundary condition (BC), inlet velocity and pressure outlet were fixed. Initial temperature conditions were set at the inlet and outlet. A saturated air stream was supplied at the inlet of the domain. The periodic boundary condition was applied to the upper and lower bounds of the domain.

Primary water droplets were injected as a form of the parcel at the left boundary of the domain presented in Fig. 1. One parcel was emitted at every time step and from each mesh. For single size droplet cases, a total of 102 parcels was emitted in every cycle from the inlet surface consisting of 102 surface elements. Given the amount G of the mass flow rate of water droplets and the number of parcels emitted P, the number of droplets m in a parcel is $G/\left(P\frac{4}{3}\pi r^3\rho_l\right)$.

For cases of distributed droplet diameter, the Rosin–Rammler distribution [9] was adopted. In computations, the distribution was discretized using a set of 20 diameters between 0.01 and the assumed maximum size. Typically a parcel per individual diameter was allocated. Consequently, 2040 (=20×102) parcels were emitted per time step from the inlet in the multi-dispersed case.

Secondary water droplets were released from points near the trailing edge of IGV using calculations of the amount of water attachment on the IGV surface. To obtain sufficient statistical results, number of water droplets emitted per a time step was ten.

In this condition, transient calculations were executed. This is the state condition. Typically, 5000 cycles were sufficient to attain convergence, which was judged as the point at when the erosion rate maintained the steady state stably. Then, an additional 80 cycles were run for erosion data sampling. That is equivalent to the time for the rotor to move two pitches circumferentially. Simulations were conducted on a personal computer (3.40 GHz Core™ i7, Intel Corp.; 16 GB RAM memory; Windows 7, Microsoft Corp.).

Erosion model

The diameter of the primary droplets entering the compressor was set to 18 μm as a typical value expected during inlet fogging operations. That of the secondary droplets emitted from IGV was 100 μm [4].

To model water impingement erosion, Itoh's empirical correlation was adopted as derived from experiments using water droplets with 100–270 μm diameter. Their observations show that erosion has three periods: incubation, transience, and steady state. In the steady state, with which we are concerned, the erosion depth is proportional to the number of droplets impacting the material. Itoh's steady state part of the erosion depth correlation is

$$E_{st} = a + b\tau \tag{1}$$

$$a = 0.541 \cdot V^{1.41} D^{1.42} H^{-1.09} \tag{2}$$

$$b = const \cdot V^{g_1(D,H)} D^{2.75} H^{9.77} N \tag{3}$$

$$g_1(D,H) = 19.5 + 0.386 \log_{10} D - 4.64 \log_{10} H, \tag{4}$$

where E_{st}(mm) and τ(hr) respectively denote the erosion depth and the time of exposure by water impingement. Parameters V(m/s), D(mm), H(-), N(1/mm^2/hr) respectively signify the impact velocity, droplet diameter, Vickers hardness of the material, and the number density of the collision rate. Here, *const.* is the

following.

$$const = 3.57 \times 10^{-53} \quad (5)$$

Above constant has a value different from that of original Itoh's equation because of following reason. Itoh's correlation is known to fit data from large size droplets around the order of 200 μm. Unfortunately, however, both the value and the unit of the number density of the collision rate N were not clearly stated in Itoh's experiment [2]. Then incorporating Tsubouchi's method N(1/mm^2/hr) was estimated by using V(m/s), D(mm) and surface area of specimen(mm^2). As a result of fitting Itoh's data, the constant shown in Eq.(5) was obtained with the other parts of Itoh's correlation unchanged. The accuracy of the correlation stated above was examined by the experiments of both Tsubouchi and Itoh.

The test piece material was 12Cr stainless steel. Experimental ranges were H=235–520, V=400–629 m/s, and D=32–269 μm. Good agreement was obtained as depicted in Fig. 3. The droplet diameters include almost all diameters that might be expected in primary and the secondary droplets in inlet fogging. For more details, Figs. 4 and 5 respectively exhibit the dependency of droplet diameter and impact velocity. Parametric trends are largely simulated.

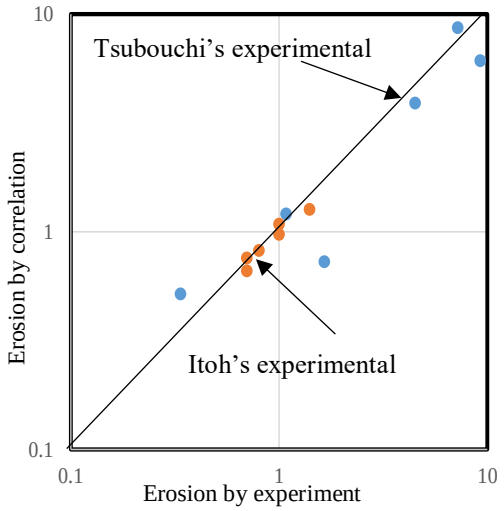

Fig. 3 Erosion by Tsubouchi's and Itoh's experiment compared with empirical correlation (unit: mm)

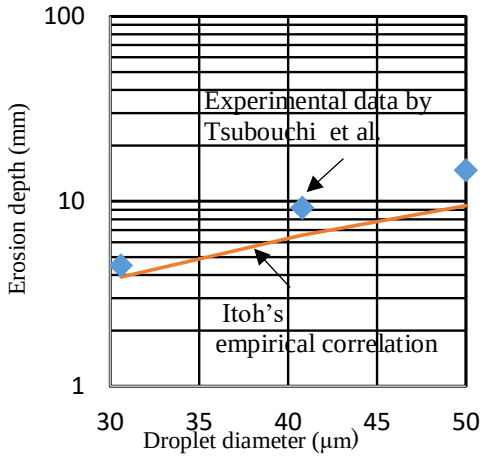

Fig. 4 Dependency of erosion depth on droplet diameter

Parcel approximation algorithm

Impacting droplets have different diameters, velocities, and impact angles. To treat this phenomenon, a parcel approximation algorithm was used. A parcel is a group of droplets having identical properties. Erosion calculations were done parcel-wise instead of using individual droplets, as described below.

(1) The number of parcels hitting a specified surface element of a blade in a sampling time t is denoted by L. Each parcel numbered by l contains m_l water droplets of the same property.
(2) In the calculation, impact velocity V is replaced by its normal component V_n.
(3) From Eqs. (2) and (3), a and b were approximated as

$$b = \frac{1}{t}\sum_l^L b_l \quad (6)$$

$$b_l = const \cdot V_{n,l}^{\,g_1(D_l,H)} D_l^{2.75} H^{9.77} m_l \quad .$$

If all the droplets are identical, then

$$N = \sum_l^L m_l / t$$

holds. Regarding a in Eq. (3), the weighted average by the number of impact droplets gives the equations shown below.

$$a = \sum_l^L a_l \cdot m_l \Big/ \sum_l^L m_l \quad (7)$$

$$a_l = 0.541 \cdot V_{n,l}^{\,1.41} D_l^{1.42} H^{-1.09}$$

In this way, distributed properties of droplets were considered in the computation of water impingement erosion.

Break-up model

Water droplets induce self-induced vibration when a velocity difference exists between the air and droplet. The water droplet might break up if the droplet Weber number ($We=\rho_l u^2 D/\sigma$) exceeds the critical Weber number (We,cr). Actually, Fluent adopts the TAB (Taylor Analogy Breakup) model [10] to address this phenomenon. From the TAB model, the analytical expression of We,cr can be derived as

$$We,cr = \frac{2C_k C_b}{C_F} / (1 + \exp(-(\frac{\pi}{\omega t_d})) \quad , \quad (8)$$

where

$$\omega^2 = C_k \frac{8\sigma}{\rho_l D^3} - \frac{1}{t_d^{\,2}}, \frac{1}{t_d} = \frac{2C_d \nu_l}{D^2},$$

$$C_b = 0.5, C_k = 8, C_d = 5, C_F = \frac{1}{3} \quad .$$

Using water property values at 20°C, ρ_l=998,2 kg/m^3,

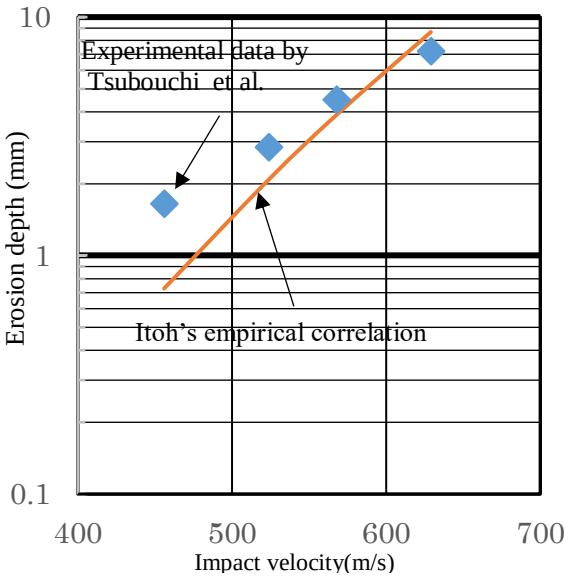

Fig. 5 Dependency of erosion depth on impact velocity

ν_f=1.004×10^{-6}m^2/s, σ=74×10^{-3}N/m and droplet diameter D of 18×10^{-6}m, We,cr will become 12.6. This value is less than the value of 30 that Tsubouchi [1] reported for a steam turbine blade, but it is close to Flock's observation [13].

Using the Weber number definition, the range of break-up of a droplet was derived as a function of diameter D and relative velocity u. Figure 6 presents the result. For example, given a droplet with D=18 μm, velocity greater than 210 m/s is needed for break-up to occur.

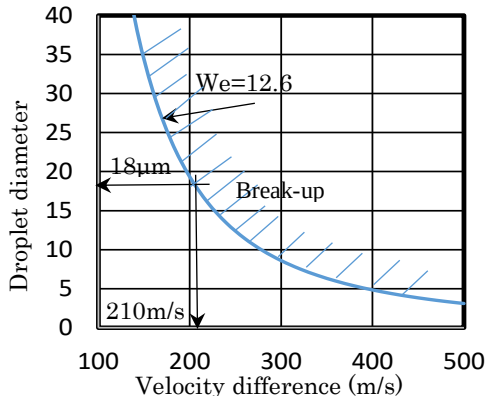

Fig. 6 Break-up area of droplet

RESULTS

Flow around blade lines

To calculate air flow the following boundary conditions were set. Inlet total pressure, outlet static pressure and moving velocity of rotor were 100126 Pa, 92762 Pa and 392.7 m/s respectively. In advance one dimensional axial flow model equivalent to the present two dimensional model was calculated [11]. Above boundary conditions were referred to the results.

The velocities of air and water droplet parcels at the inlet were set to the same velocity of inlet air. The droplet diameter was 18 μm, with water to air mass ratio of 0.63% referring to reference [11]. Figure 7 shows the static pressure contour as a function of the deviation from atmospheric pressure. Pressure becomes negative at the rotor blade bottom surface and positive at the leading edge and upper surface. Velocity distributions are shown in Fig. 8(a) and (b). Figure 8(b) depicts the sudden change in the velocity vector near the leading edge and thin boundary layer was made near leading edge. Calculated inlet velocity became 152.8m/s which was approximately equal to predicted value 143m/s by one dimensional axial flow model. Therefore these results are reasonable.

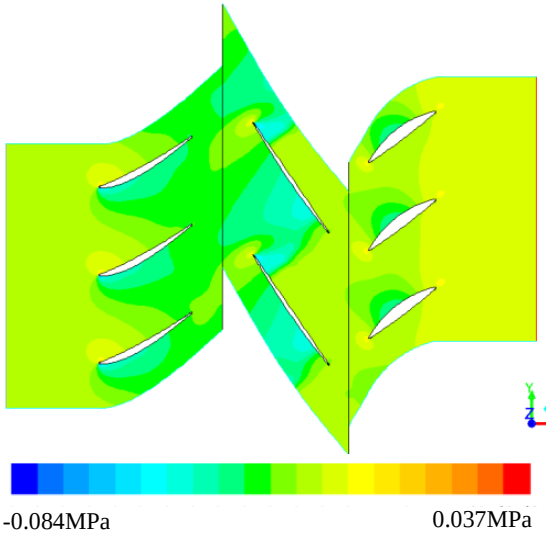

Fig. 7 Static pressure distribution (relative value)

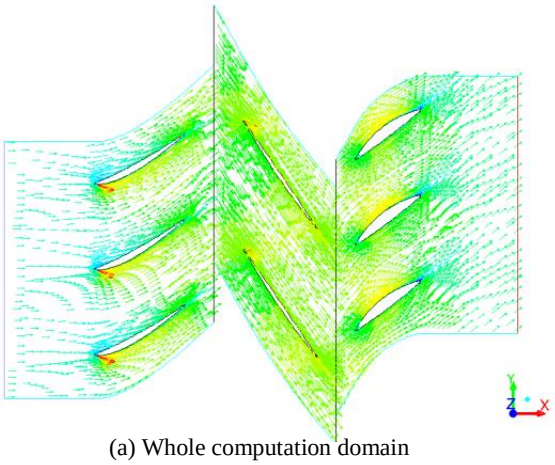

(a) Whole computation domain

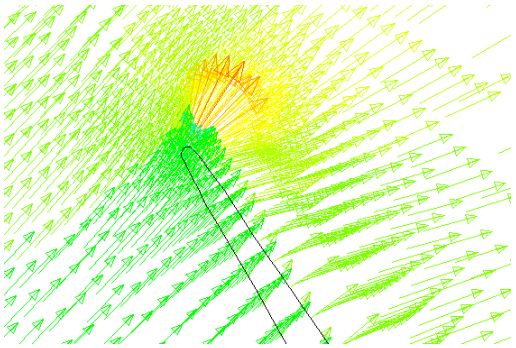

(b) Around leading edge of rotor

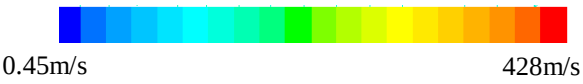

Fig. 8 Velocity distribution

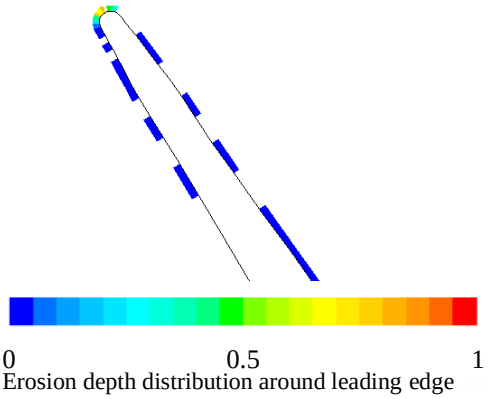

(a) Erosion depth distribution around leading edge

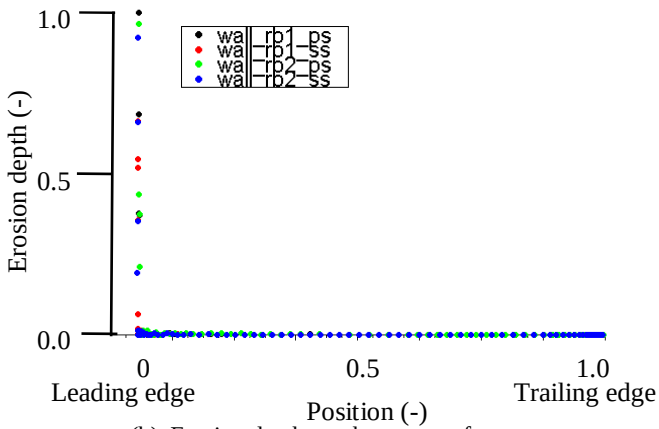

(b) Erosion depth on the rotor surface

Fig. 9 Erosion along the rotor surface by single size primary droplets in the case of inert and without break-up

Validation of parcel approximation with single-size droplets

Validation is needed for computation results obtained by parcel approximation algorithm to ascertain if they are equal to those obtained using Itoh's empirical correlation. To this end, the case of single size droplets with neither break-up nor evaporation to which Itoh's correlation can be directly applied was taken. As shown in Fig. 9(a) erosion is found to be localized at the element near the leading edge of rotor with the impact angle 90 deg ($V=V_n$). Figure 9(b) presents the profile of erosion depth of the primary droplet of 18 μm against distance from the leading edge to the trailing edge. The erosion depth is normalized by its maximum at the leading edge. This unit will be applied hereinafter. Black and green dots exhibit erosion on the pressure side of blades 1 and 2. Red and blue are those of the suction side. No significant difference was found between rotors 1 and 2, which proves that the computational geometry and the given periodic boundary condition are proper.

Maximum erosion depth appearing at the leading edge of the rotor was selected for validation of the parcel approximation algorithm. Table 1 compares Fluent solution with Itoh's direct calculation for primary and secondary droplets. The unit of erosion depth is relative to the Fluent solution for the 18 μ m primary droplets shown in Fig. 9. Itoh's calculation was executed using the values N and V_n that Fluent calculated. Agreement between the two was obtained and the algorithm validated.

Behavior of primary droplet with the break-up model

Spatial distribution of the droplet size was calculated under the condition that the steady state was reached. 18 μm single-size droplets were injected with the break-up model examined here. The maximum erosion depth decreased considerably to 0.1. The reason for this reduction was investigated. Figure 10 presents the

Table 1 Verification of parcel approximation algorithm

Operation condition	Unit	Primary droplets	Secondary droplets
Diameter D	μm	18	100
Number ratio of impact droplets N	$1/m^2/s$	1.73E+12	9.25E+10
Velocity Vn	m/s	320	330
Vickers hardness H	—	350	350
Operation time	hr	2000	2000
Itoh's correlation(5)	(-)	1.02	6.96
Solution of FLUENT (6),(7)	(-)	1.00	6.69

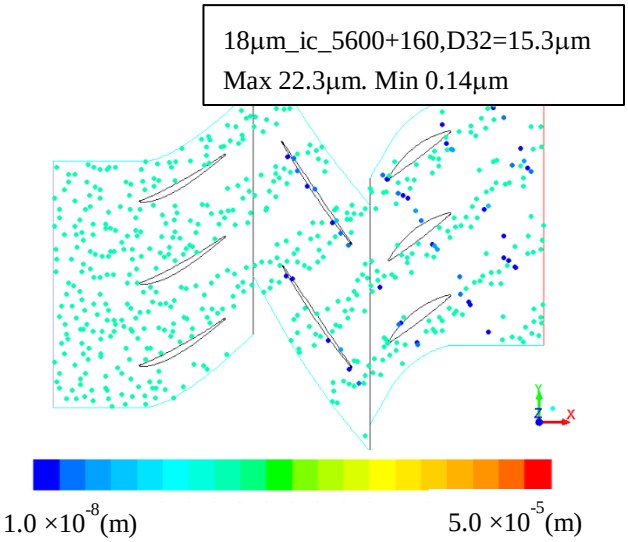

Fig. 10 Droplet size distribution in computational domain

spatial distribution of the droplet size in the domain. A group of small droplets (dense blue) is seen to flow down along the rotor blade surface. Droplet break-up is thought to occur around the leading edge of the rotor. Smaller droplets are produced. Most are likely to move together with the air stream along the blade. Some, however, collide with the leading edge. To examine this phenomenon, the droplet size distribution at exits of the IGV, rotor blade (rb), and the stator blade (sb) was calculated.

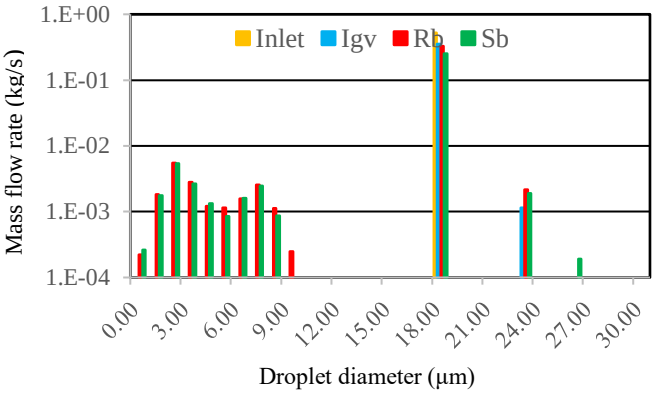

Fig. 11 Droplet distribution at blade exit

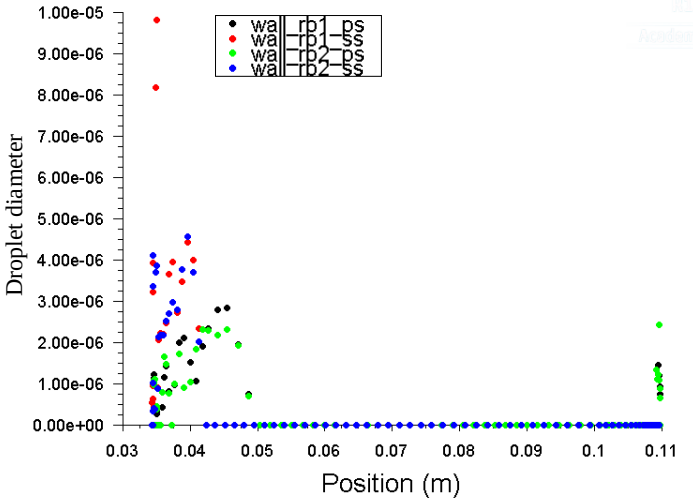

Fig. 12 Average diameter of impact droplets

Figure 11 shows that 4.3% of initial droplets disappear at rb. This results from break-up because Fig. 12 portrays that the size of droplets impacting leading edge is less than 10 μm. Next, the amount of impinging droplet mass was evaluated. In the computation, a droplet disappears once it attaches to a wall. As presented in Fig. 13, an extremely small amount of them, 0.9%, impact the rotor blade. Therefore, 20% (=0.9/4.3) of smaller droplets resulting from break-up impact the rotor wall. For that reason, less erosion depth is obtained with the break-up model.

Moreover, about 30% of the primary droplets are seen to be trapped by IGV, which is the source of the generation of the secondary droplets. The pass-through ratio of the first stage (rb+sb) becomes 77%, which coincides with Myoren's result [11]. Therefore, the present analysis was judged as valid.

Secondary droplet with size distribution

Based on the result presented in Fig. 13, 30% of the injected mass of droplets was released as secondary droplets at the trailing edge of IGV. A water film flow are made by air flow along the surface of IGV and separate from surface at trailing edge. The film breaks into many droplets. And these droplets break up finer droplets. The size of droplets become about 100 μm reported in the literature [4]. Therefore droplets with the size distribution were assumed for average diameter (D32) of 100 μm. It was emitted

with a speed of 120 m/s. Figure 14 depicts spatial distribution of the secondary droplets at an instance. In the case of figure, released droplet size and timing from each IGVs were given at random according to Rosin–Rammler distribution. The droplet trajectory meets the rotor blade intermittently. Smaller droplets are produced because of the break-up. Different from the primary droplets, smaller droplets were produced by break-up flow in the same direction as that of the initial velocity vector. That phenomenon might be attributable to inertia force greater than that of the primary droplet because of the larger diameter in this case.

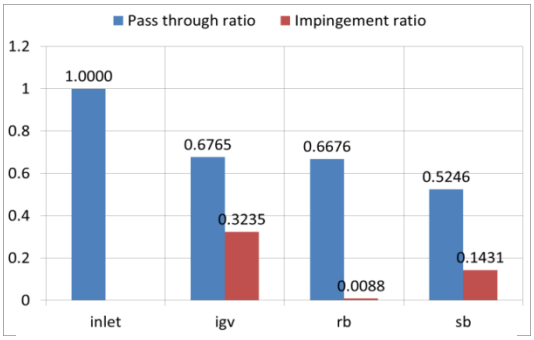

Fig. 13 Mass ratio of droplet impingement.

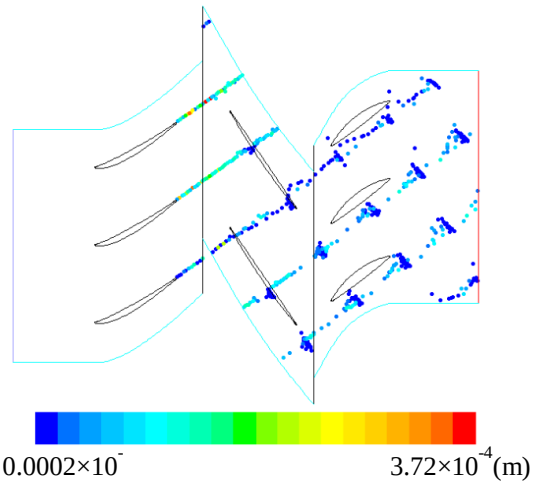

Fig. 14 Distribution of droplet diameter in space in the case of secondary droplet

Erosion depth evaluation

The maximum erosion depth caused by primary droplets was found at the leading edge of the rotor blade among surfaces present in the whole computational domain. We define the reference case as characterized by 18-μm single-sized droplets, inert (without evaporation), and without a break-up model. Then we use the unit of the erosion depth so that the maximum of the reference is unity as described in earlier section.

Pressure side erosion is more intensive than suction side erosion. For droplets with a size distribution and having the same D32 as Fig. 9, the maximum erosion depth was 0.96, which was almost equal to the value of unity in the case of single-sized droplets. From this fact, it can be concluded that the present parcel approximation algorithm is applicable to a polydispersity system.

Next, parametric effects were identified. They are (1) monodispersity / polydispersity, (2) inert / evaporative, and (3) break-up / without break up. Table 2 presents the maximum erosion depth. The break-up mechanism reduces erosion to 1/12–1/5 of that without break-up. Evaporation reduces erosion to 1/3–3/5 of that of the inert case. In the case of Polydispersity in table 2, spread parameter and mean diameter of Rosin–Rammler parameter were set to 3.235 and 23.62 μm respectively.

Figure 15 portrays the erosion distribution by secondary droplets with 100 μm diameter. Two distinct features that differ from primary features are observed. First, in spite of less mass flow, severe erosion exists by 6.7 times more than that of the primary. The effect of larger initial droplet size supersedes the negative effect of the lesser mass flow. Marked erosion was expected to occur at widely various pressure sides of the blade surface. Even though large droplets break up, their eventual size is not sufficiently small to avoid erosion. Results show that the secondary droplet, rather than the primary droplet, governs erosion. With the present break-up model, however, the maximum reduces to 0.7, about one-tenth of the case without break-up.

Table 2 Summary of erosion depth by primary droplet (unit : relative)

		Monodispersity	Polydispersity
Without break-up	Inert	1.00	0.96
	Evaporation	1.08	0.62
Break-up	Inert	0.10	0.08
	Evaporation	0.20	0.07

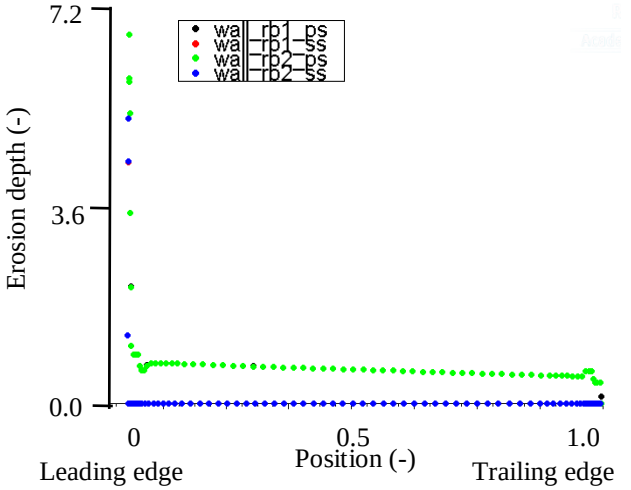

Fig. 15 Erosion along the rotor surface by single size secondary droplets in the case of inert and without break-up

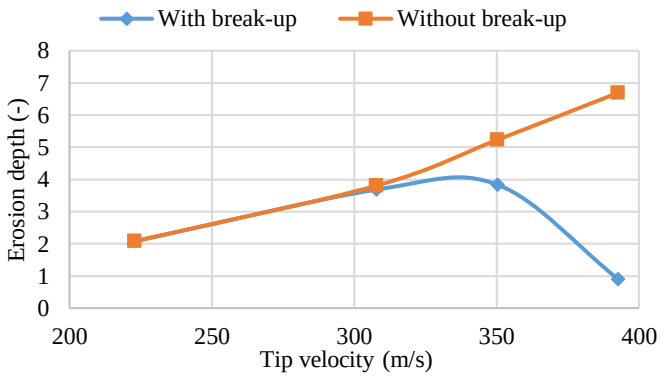

Fig. 16 Influence of rotor speed on erosion

Effect of rotational speed

Figure 16 presents erosion depths at the leading edge as a function of the rotor speed. With the break-up model (blue line) there exists a velocity that gives a maximum. The erosion depth increases with velocity in a low speed range where $We < We,cr$ holds. After a certain velocity where $We = We,cr$ holds, the droplet starts breaking up. The higher the velocity, the finer the droplet size becomes as a result of sequential break-up. From this observation, the erosion depth at the leading edge varying in the span direction is expected to have a profile with a trend coinciding with the field data [12]. In vacuum environment, like in steam turbine, no shear stress is applied to droplets. Therefore in the case of steam turbine water droplets collide to the rotor without break-

up. As a result, the erosion of steam turbine blade increases with velocity. In this point, the erosion behavior of the steam turbine is different from that of gas turbine compressor whose pressure is atmospheric at inlet. .

DISCUSSION

Influence of the critical Weber number on erosion

Droplet break-up might occur near the trailing edge of the rotor blade, where abrupt change in the velocity vector of air occurs as well as acceleration because of centrifugal force. The critical Weber number (*We,cr*) of the droplet determines the maximal stable droplet diameter in an air stream. To ascertain the proper value of *We,cr* under such circumstances, two reports of the literature were surveyed. Their sensitivity to erosion depth was examined.

According to the TAB model [10] as described in the foregoing section, *We,cr* for a droplet with temperature of 20°C is 12.6. This fact coincides with Flock's experiment [13] demonstrating that bag-type break-up occurs for droplets floating in the air stream in the range of $9<We<15$. Hamitt et al. [14] surveyed experimental data obtained by several researchers related to the break-up and subsequent fragmentation of a water film formed on a plate installed parallel to the air stream. They correlated *We,cr* data against the Mach number, which Matsuzaki et al. [5] formulated as function of Mach number *M* as follows.

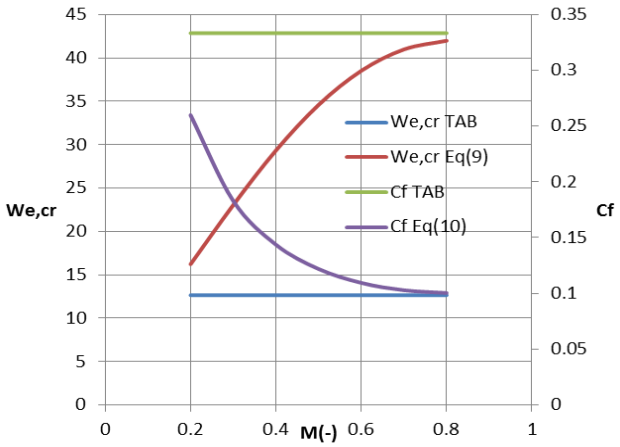

Fig. 17 Critical Weber number and Cf as function of Mach number.

Table 3 Maximum erosion depth under different critical Weber number

Model	Cf	Erosion depth (-)
Without break-up	-	6.7
With break-up	0.333	0.904
	Eq.(10)	6.7

$$We,cr = -25.824M^5 + 132.19M^4 - 234.51M^3 + 118.76M^2 + 45.365M + 4.074 \quad (9)$$

To make Eq. (9), the built in Fluent calculation C_F value in Eq. (8) was replaced by

$$C_F = -4.4113M^5 + 13.483M^4 - 16.676M^3 + 10.729M^2 + 3.7482M + 0.6936 \quad (10)$$

Figure 17 shows Eqs. (9) and (10) in comparison with the TAB model. The TAB model appears to have an upper and lower bound of Eqs. (9) and (10), which approaches the TAB model at low Mach number. For $M>0.2$, Eq. (9) gives a higher value of *We,cr*, which means that it is unlikely to break up. Taking 100 μm single-sized secondary droplet without the break-up model, the break-up area was obtained and compared between two models of *We,cr*. Figure 18 shows regions satisfying $We>We,cr$ in red, where the break-up might occur for Eq. (10) and C_F=1/3(TAB model). Clearly, Eq. (9) gives a narrower break-up region where the minimum value of Eq. (9) was 27.7.

Table 3 presents erosion depths for both cases. For Eq. (10) giving C_F=0.147 near leading edge, the maximum erosion depth is the same as that without a break-up model. To clarify the reason, we investigated the break-up time from the beginning of deformation until the separation and creation of smaller droplets.

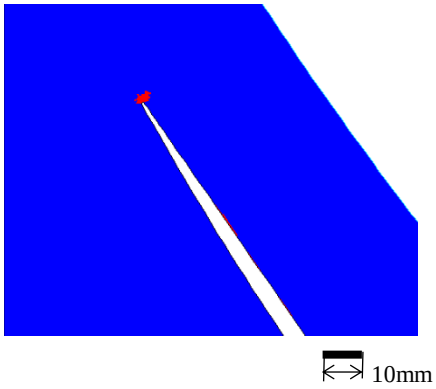

(a) In the case of We,cr calculated by Eq.(10)

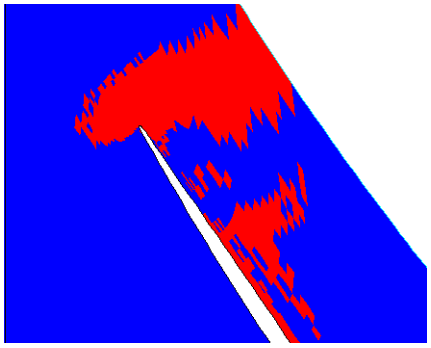

(b) In the case of We,cr using TAB model

Fig. 18 Break-up area around rotor leading edge under different critical Weber number (Drop diameter of 100μm)

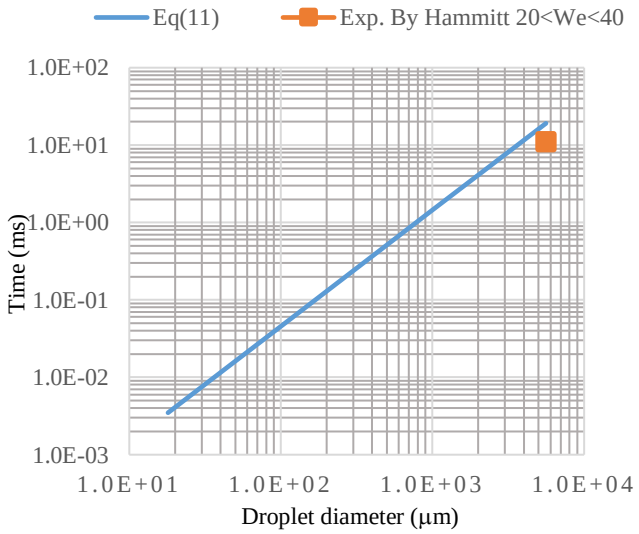

Fig. 19 Break-up duration vs droplet diameter

Break-up time consideration

From Eq. (8), the break-up time for the droplet on the verge having a critical Weber number is derived as shown below.

$$t = \frac{\pi}{\omega} = \pi \Big/ \sqrt{C_k \frac{\sigma}{\rho_l r^3} - \frac{C_d^2}{4}\left(\frac{v_l}{r^2}\right)^2} \tag{11}$$

Figure 19 presents the break-up time by Eq. (11) against the droplet diameter. The experiment examined an average of data executed at 20<*We*<40. Good agreement was found for droplets of 5.6 mm diameter. Extrapolation of this to 100 μm gives 50 μs. Assuming impact velocity of 300 m/s, then the length of flight becomes 15 mm ($=3 \cdot 10^5 \times 5 \cdot 10^{-5}$), which is greater than the greatest distance in the red area from the leading edge in the upper panel of Fig. 18. This fact implies that break-up does not finish at the time of impingement, even though it has started. For that reason, the erosion depth is the same as the case of the non-break-up model. Figure 20 shows that the impact droplets maintain the initial diameter at the leading edge

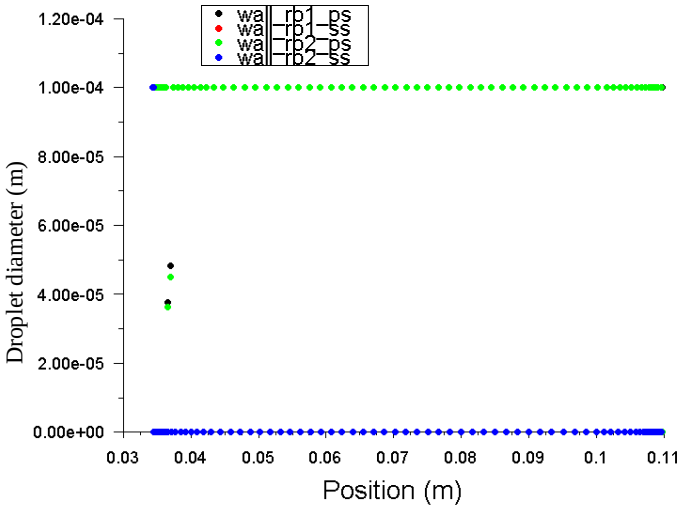

Fig. 20 Average diameter of impact droplets

CONCLUSIONS

Water droplet behavior during inlet fogging operations in an axial flow compressor of a gas turbine was investigated numerically. The geometry configuration included Inlet guide vane (IGV) and the first stage rotor and stator. Special emphasis was placed upon evaluation of the secondary droplet mass flow, multi-disperse droplet characteristics, and droplet break-up events. Simulation was executed using ANSYS Fluent® v.16.1. The following results were obtained.

(1) Numerical calculations using representative diameter D32 are appropriate under the condition that no diameter change occurs during flight. A new algorithm was developed to accommodate droplets of various diameters attributable to break-up or evaporation in erosion evaluation.

(2) Erosion depth by the impingement of the secondary droplets emitted from the trailing edge of IGV is much greater than that by the primary droplet, although the mass is less in the secondary droplets.

(3) Break-up of droplets might occur near the leading edge of the rotor due to shear force from ambient air, producing smaller droplets, which suppresses blade erosion if the rotor blade rotational speed is sufficiently high. Therefore, certain speed exists that gives rise to maximum erosion depth. This erosion mechanism is unique in compressor and is different from that of steam turbine installed in vacuum environment where the break up is hard to occur.

(4) The speed above depends greatly on the choice of the value of the critical Weber number.

To date, knowledge related to the critical Weber number has been obtained experimentally in a simple steady state flow field. However, the flow field near the rotor leading edge is a spatially accelerating flow field that is complex where a hidden parameter might exist for the break-up. Therefore, further experimental and theoretical study is strongly recommended as future work.

ACKNOWLEDGMENTS

This research was supported financially by the Ministry of Economy, Trade and Industry of Japan, Agency for Natural Resources and Energy. The authors wish to express their deep gratitude. They are also indebted to Dr. Kuniyoshi Tsubouchi for valuable discussions.

REFERENCES

[1] K. Tsubouchi, N. Yasugahira, S.Yoshida, R.Kaneko, T. Sato, 1990, An Evaluation of Water Droplet Erosion for Advanced Large Steam Turbine, *Advances in Steam Turbine Technology for Power Generation*, PWR-Vol. 10,ASME, Book No. G00518

[2] Itoh, H., Okabe, N., 1993, Evaluation of erosion by liquid droplet impingement for metallic materials (in Japanese), *Transactions of JSME (a),* Vol. 59, No. 567, pp. 2736-2741.

[3] Hattori, S., Kakuichi, M., 2012, Effect of impact angle on liquid impingement erosion (in Japanese), *Transactions of JSME (a),* Vol. 78, No. 791(-7), pp. 1023-1032.

[4] Uchida, T., Ootomo, F., Fukutake, H., Itoh, M., Kanome, H., Okuno, K., 2014, Behavior of droplets atomized from the air cooled-gas turbine inlet guide vane trailing edge and erosion evaluation of compressor blades (in Japanese), *GTSJ Journal*, Vol. 42, No. 3, pp. 214-219.

[5] Matsuzaki, Y., Nakano, S., Toriyama, H., Takeda, Y., Satou, K., 2015, A study of disruption patterns of water film splashed into air flow (in Japanese), *GTSJ Journal*, Vol. 43, No. 6 (.11), pp. 451-457.

[6] Suzuki, M., Yamamoto, M., 2014, Numerical simulation of liquid droplet impingement erosion (in Japanese), *Proceeding 42nd Meeting of GTSJ*, A-20.

[7] Suzuki, M., Yamamoto, M., 2015, Numerical analysis of liquid droplet impingement erosion on compressor cascade (in Japanese), *Proceeding 43rd Meeting of GTSJ*, C-15.

[8] Hamdani, A., Utamura, M., Shibata, T., Myoren, C., 2015, Numerical simulations of droplet coalescence in an L-shaped duct for inlet fogging of gas turbine engines, *International Journal of Gas Turbine, Propulsion and Power Systems*, Vol. 7, No. 1.

[9] Lefebvre, A. H., 1989, Atomization and sprays, *Hemisphere Publishing Corporation.*

[10] P. J. O'Rourke, A. Amsden, 1987, The TAB Method for Numerical Calculation of Spray Drop Breakup, *SAE Paper*, No. 872089.

[11] C. Myoren, Y. Takahashi et al., 2013, Evaluation of Axial Compressor Characteristics under Overspray Condition, *Proceedings, ASME Turbo Expo 2013*: Turbine Technical Conference and Exposition GT2013.

[12] Gajjar, H., Chaker, M., Dighe, A., Homji, C. M., 2003, Inlet fogging for a 655 MW combined cycle power plant-design, implementation and operating experience, *Proceedings ASME Turbo Expo 2003*, GT2003-38757.

[13] Flock, A.K., Guildenbecher, D.R., Chen, J., Sojka, P.E., Bauer, H.J., 2012, Experimental statistics of droplet trajectory and air flow during aerodynamic fragmentation of liquid drops, *International Journal of Multiphase Flow*, Vol. 47, pp. 377-49.

[14] Hammitt, F. G. Kreczkowski, S. and Krzyzanowki, J., 1981, Liquid film and droplet stability consideration as applied to wet stream flow, *Forschung. Ing-Wes*, 47.